A Delaunay-based Coordinate-free Mechanism for Full Coverage in Wireless Sensor Networks

Chenxi Qiu
Dept. of Electrical and Computer Engineering
Clemson University
Clemson, USA
chenxiq@clemson.edu

Haiying Shen
Dept. of Electrical and Computer Engineering
Clemson University
Clemson, USA
shenh@clemson.edu

***Abstract*—Recently, many schemes have been proposed for detecting and healing coverage holes to achieve full coverage in wireless sensor networks (WSNs). However, none of these schemes aim to find the shortest node movement paths to heal the coverage holes, which could significantly reduce energy usage for node movement. Also, current hole healing schemes require accurate knowledge of sensor locations; obtaining this knowledge consumes high energy. In this paper, we propose a DElaunay-based Coordinate-free Mechanism (DECM) for full coverage. Based on rigorous mathematical analysis, DECM can detect coverage holes and find the locally shortest paths for healing holes in a distributed manner without requiring accurate node location information. Simulation results and experimental results from the real-world GENI Orbit testbed show that DECM achieves superior performance in terms of the energy-efficiency and effectiveness of hole healing compared to previous schemes.**

***Keywords*-wireless sensor networks; coverage holes; node movement; energy usage;**

I. Introduction

In wireless sensor networks (WSNs), sensor nodes may die due to battery drain or environmental causes. Also, nodes may deviate from their assigned positions due to the effects of uncontrollable factors (e.g., ocean waves). Coverage holes hamper the ability of WSNs to detect events and reduce network reliability. Therefore, it is crucial to equip the sensor nodes with efficient hole detection and healing capabilities in order to ensure full coverage of the target field.

Numerous schemes have been proposed for healing coverage holes in WSNs. Many of these [1]–[13] leverage sensor movement to improve network coverage. Since mechanical movement is much more energy-expensive than electronic communications [14], the node moving distance should be minimized [15]. However, none of the previous hole healing works aim to find the shortest paths of node movement, which could greatly enhance the energy-efficiency. Also, all of these schemes require accurate knowledge of node locations. However, simple localization solutions, such as equipping each node with a GPS receiver or manual configuration using coordinates [4], [16]–[18], are either energy-expensive or impractical for WSNs in some cases [19].

To overcome the drawbacks, we propose a DElaunay-based Coordinate-free Mechanism (DECM) for full coverage in WSNs. Based on rigorous mathematical analysis, DECM can find the locally shortest paths for node movement in healing coverage holes in a distributed manner without accurate location information.

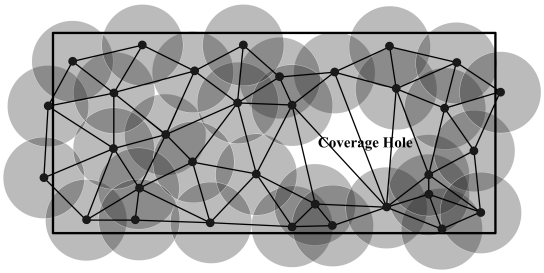

Figure 1. Delaunay triangulation.

In this paper, we first present a mathematical model that provides a sufficient and necessary condition for the full coverage of a triangle that has no other nodes inside its circumcircle. DECM is a distributed scheme in which every node checks for holes and makes movements to heal holes. As shown in Fig. 1, each node first conducts Delaunay triangulation that divides the target field into triangles that have no other nodes inside. Then, based on the sufficient and necessary condition, each node calculates the its safe area where the node can be located while still keeping full coverage of its triangles. Based on the calculated safe areas of each node, DECM can detect coverage holes and find the shortest paths for node movement to heal the holes. DECM utilizes the r-map coordinate system [20] to enable nodes to know the relative locations of nearby nodes for hole detection and healing.

DECM is similar to a Voronoi diagram based method (VOR) [7] since both construct a diagram for hole healing. VOR forms a WSN into Voronoi cells, each of which has one sensor called a *generating node* residing in it. All points within a Voronoi cell are closer to their generating node in the cell than to those in other cells. Thus, if a generating node finds some points in a Voronoi cell that are not covered by itself, it moves directly to the farthest point to heal the hole. However, VOR may generate numerous iterations of node movements because (1) node movement to cover one point rather than the cell area may generate holes in other points in the cell, and (2) only one node is in charge of the coverage of a cell. Unlike in VOR, a node in DECM moves to a point in order to cover the entire area of a Delaunay cell. Also, three nodes are in charge of the coverage of a cell. Thus, DECM achieves full coverage more quickly and

energy-efficiently.

This paper is organized as follows. Section II presents a concise review of related works on movement-assisted schemes for full WSN coverage deployment. Section III introduces mathematical models for analyzing WSN coverage problems and presents the DECM movement-assisted scheme for detecting and healing coverage holes based on this model. Then, Section IV presents a performance evaluation of DECM in comparison with several previous schemes. The final section concludes with a summary of contributions and a discussion on further research work.

II. Related Works

Node movement strategies for full area coverage have gained considerable attention during recent years. In virtual force methods [6], [8]–[10], sensors are likened to electromagnetic particles and have repulsive and attractive forces between them. When the distance between two sensors is too great, the attractive force makes them pull each other closer; when the distance is too small, the repulsive force makes them push each other further away. Consequently, sensor nodes are exploded from dense regions to sparse regions or holes. However, these methods require sensors to move over a series of iterations to balance "virtual forces" between themselves, which may take a long time to converge and is not practical for real applications due to the high energy cost of node movement.

Wang *et al.* [7] used the Voronoi diagram for healing coverage holes. As explained in the previous section, in these methods, a node's movement cannot completely heal the coverage holes in its Voronoi cell because one hole healing may produce other holes in its Voronoi cell, subsequently generating many iterative node movements.

Many grid quorum-based movement schemes [1]–[5] view the movement-assisted network re-deployment problem as a load balancing problem under the virtual grid model [21]. These schemes partition an entire target region into small grid cells, and consider the number of nodes in each cell as the cell's load. The schemes schedule sensor movement in order to achieve a balanced load distribution among the grid cells. A node within a grid cell can directly communicate with other nodes in its four adjacent cells and makes movement decisions according to information from adjacent cells. Some of these schemes also try to minimize the sensor movement distances. For example, SMART [5] arranges communication between cell heads to identify overloaded and underloaded cells and direct nodes from overloaded cells to move to underloaded cells. Knowing the loads of other cells, each cell tries to avoid any unnecessary movement; thus, both the total moving distance and the total number of moves can be minimized. However, since the target a node moves to is a cell rather than a specific point, the schemes still cannot find the shortest moving paths.

There are other movement-assisted methods using different strategies. Luo *et al.* [15] assumed that the entire target region is fully covered initially, and each node dominates a number of interest points which are randomly and uniformly distributed throughout the entire region. When some nodes lose their interest points, their neighbors move to inherit them. Heo and Varshney [13] proposed an intelligent energy-efficient deployment algorithm for cluster-based WAN by synergistic combination of cluster structuring and a peer-to-peer deployment scheme. Zhang and Arora [12] proposed the GS^3 algorithm for multi-hop wireless networks. The algorithm enables nodes in a 2D plane to configure themselves into a cellular hexagonal structure such that cells have tightly bounded geographic radii and low overlap between neighboring cells. Butler and Rus [11] proposed an approach for positioning and organizing mobile sensors in response to events in their environment.

Admittedly, the above movement-assisted schemes have their own merits. However, all of these schemes require nodes to have accurate location information. Though Bejerano *et al.* [20] proposed a locality-free scheme, it is for hole detection rather than for hole healing. Also, none of these schemes aim to find the shortest movement paths only using local location information. DECM can find the locally shortest moving paths for healing coverage holes in a distributed manner without accurate location information.

III. The Design of DECM

We consider a WSN comprised of numerous mobile nodes that are uniformly distributed over a large *target field* and are designed to detect specified events. Each node, denoted s, can sense specified events in its *sensing range*, denoted by R_s.

We first find the condition for full coverage of a triangle formed by three sensors with no other nodes inside the triangle's circumcircle (Section III-A). Since a Delaunay triangle has no other nodes inside the triangle's circumcircle, nodes conduct Delaunay triangulation [22] to divide the field into Delaunay triangles (Section III-B). Then, each node uses our observed full coverage condition to find a safe area where it can be located while still keeping full coverage of its triangles (Section III-C). Finally, each node can detect holes and discover the shortest path for its movement to heal holes (Section III-D).

A. Condition for A Triangle's Full Coverage

Consider three nodes in a plane that construct a triangle. The sufficient and necessary condition for the triangle's full coverage is described in *Theorem 3.1*.

Theorem 3.1: Consider a triangle formed by three nodes s_i, s_j and s_k with no other nodes placed inside the triangle's circumcircle. Using d_{ij} to denote the distance between s_i and s_j, and with the same convention for the other distances, we derive:

1) when the triangle is an acute triangle, the triangle is fully covered iff the following condition is satisfied:

$$R_s \geq \frac{d_{ij}d_{jk}d_{ik}}{\sqrt{\left(d_{ij}^2+d_{ik}^2+d_{jk}^2\right)^2-2\left(d_{ij}^4+d_{ik}^4+d_{jk}^4\right)}} \quad (1)$$

2) when the triangle is an obtuse triangle, the triangle is fully covered iff the following condition is satisfied:

$$R_s \geq max\{\frac{d_{ij}^2 d_{jk}}{d_{ij}^2+d_{jk}^2-d_{ik}^2}, \frac{d_{ik}^2 d_{jk}}{d_{ik}^2+d_{jk}^2-d_{ij}^2}\} \quad (2)$$

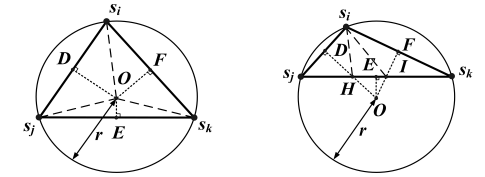

(a) Acute triangle (b) Obtuse triangle

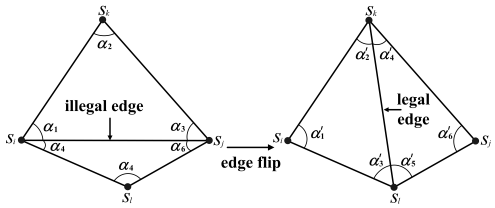

Figure 3. Illegal edge and edge flip.

Proof: Fig. 2 (a) shows an acute triangle formed by three sensor nodes. Point O is the circumcenter of $\triangle s_i s_j s_k$ and r is the radius of the triangle ($r = Os_i = Os_j = Os_k$). Obviously, if $R_s < r$, where

$$r = \frac{d_{ij} d_{jk} d_{ik}}{\sqrt{\left(d_{ij}^2 + d_{ik}^2 + d_{jk}^2\right)^2 - 2\left(d_{ij}^4 + d_{ik}^4 + d_{jk}^4\right)}},$$

point O cannot be covered by any sensor node; otherwise, every point within $\triangle s_i s_j s_k$ can be covered by at least one of the three nodes.

Fig. 2 (b) shows an obtuse triangle formed by three sensor nodes. Because the circumcenter of the obtuse triangle is outside of the triangle, $R_s \geq r$ is not the necessary condition for triangle's full coverage. In the figure, DH, FI, and EO are the perpendicular bisectors of $s_i s_j$, $s_i s_k$ and $s_j s_k$. If $R_s > Hs_i = Hs_j$, then $\triangle DHs_i$ and $\triangle DHs_j$ are fully covered. Similarly, if $R_s > Is_i = Is_k$, then $\triangle IFs_i$ and $\triangle IFs_k$ are fully covered. In $\triangle HIs_i$, either H or I must be the farthest point from s_i. Therefore, $\triangle DHs_i$, $\triangle DHs_j$, $\triangle IFs_i$, $\triangle IFs_k$ and $\triangle HIs_i$ are fully covered iff

$$\begin{aligned} R_s &\geq max\{Hs_i, Is_i\} \\ &= max\{\frac{d_{ij}^2 d_{jk}}{d_{ij}^2 + d_{jk}^2 - d_{ik}^2}, \frac{d_{ik}^2 d_{jk}}{d_{ik}^2 + d_{jk}^2 - d_{ij}^2}\}. \end{aligned}$$

■

B. Coordinate-free Delaunay Triangulation

The Delaunay triangulation [22] is used in mathematics and computational geometry.

Definition 1 (*Delaunay triangulation [22]*) A triangulation for a set S of points in a plane is a Delaunay triangulation if no point in S is inside the circumcircle of any triangle.

Based on Theorem 3.1, we first conduct Delaunay triangulation so that there are no other nodes placed inside each triangle's circumcircle. Before we present how to conduct Delaunay triangulation on a WSN, we first introduce some definitions and theorems [22].

Definition 2 (*edge flip*) [22]: As Fig. 3 shows, consider an edge $e = s_i s_j$ of a triangulation. If e is not an edge of the unbounded face, it is and incident to two triangles $s_i s_j s_k$ and $s_i s_j s_l$. If the two triangles form a convex quadrilateral, we can obtain a new triangulation $\mathcal{T}'$ by removing $s_i s_j$ and inserting $s_k s_l$ in triangulation $\mathcal{T}$. We call this operation an *edge flip*.

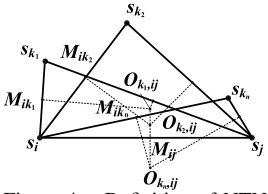

Figure 4. Definition of NTN.

Definition 3 (*illegal edge*) [22]: As Fig. 3 shows, after an edge flip, the only difference between $\mathcal{T}$ and $\mathcal{T}'$ is that the six angles $\alpha_1, ..., \alpha_6$ are replaced by $\alpha_1', ..., \alpha_6'$. We call the edge $e = s_i s_j$ an *illegal edge* if

$$min(\alpha_i) < min(\alpha_i') \quad (1 \leq i \leq 6) \tag{3}$$

Definition 4 (*legal triangulation/triangle*) [22]: A triangulation/triangle that does not contain any illegal edge.

Theorem 3.2: A triangulation for a set S of points in a plane is a legal triangulation iff the triangulation is a Delaunay triangulation [22].

The Delaunay triangulation and hole healing require each node to obtain the distances and directions of nearby nodes. For this purpose, DECM uses the r-map system [20], in which each node measures the locations of its neighbors using its own arbitrary polar-axis.

Definition 5 (*r-map* [20]): The r-map of node s_i is a variant of polar coordinates that specifies the relative location of its r-vicinity, denoted $N_{s_i}(r)$. The location of any node $s_j \in N_{s_i}(r)$ is presented as (d_{ij}, θ_{ij}), where d_{ij} is the *radial coordinate* that indicates the Euclidian distance between nodes s_i and s_j, and θ_{ij} is the *angular coordinate* of node s_j that denotes the direction of s_j relative to an *arbitrary polar-axis* of s_i.

Neighboring nodes periodically exchange their measured r-maps with their neighbors and receive r-maps. When s_i receives s_j's r-map containing the location of s_k measured by s_j, s_i can transform s_k's location to the location measured by s_i's polar-axis using the methods in [20], [23].

Definition 6 (*shared nodes*): Shared nodes of s_i and s_j are nodes that exist in both s_i's r-map and s_j's r-map.

Definition 7 (*potential edge*): A potential edge is an edge that has at least one side with no constructed triangle and with at least one shared node.

In the Delaunay triangulation algorithm, DECM first selects one node as a *seed node*. The *seed node* finds its nearest neighbor and builds an edge to it. The two nodes connected by this edge (edged nodes) choose a nearby node to form a triangle so that the triangle's circumcircle is minimized. We call this node the *nearest triangle neighbor (NTN)* of the edged nodes or the edge.

To find the NTN on one side of edge e_{ij}, two edged nodes, s_i and s_j, communicate with each other to determine their shared nodes, denoted $N_{s_j(r)} \cap N_{s_i(r)}$. Suppose $s_{k_1}, s_{k_2}, ..., s_{k_m} \in N_{s_j(r)} \cap N_{s_i(r)}$. As shown in Fig. 4, for one side of e_{ij}, all nodes $s_{k_1}, s_{k_2}, ..., s_{k_m}$ are connected with s_i (or s_j), thus generating edges $e_{k_1 i}, e_{k_2 i}, ..., e_{k_m i}$ (or $e_{k_1 j}, e_{k_2 j}, ..., e_{k_m j}$). These edges' perpendicular bisectors intersect with the perpendicular bisector of e_{ij} at point $O_{k_1,ij}, O_{k_2,ij}, ..., O_{k_m,ij}$, respectively. We use variable $h_{k,ij}$ to denote the distance between $O_{k,ij}$ and e_{ij}, i.e., $|h_{k,ij}| = M_{ij}O_{k,ij}$, where M_{ij} is the middle point of e_{ij}. If $O_{k,ij}$ and s_k are located at the same side of e_{ij}, then $h_{k,ij} > 0$; and if $O_{k,ij}$ and s_k are located at different sides, then $h_{k,ij} < 0$. Suppose $h_{k_n,ij}$ has the smallest value among $h_{k,ij}$; then s_{k_n} is the NTN of e_{ij}.

As shown in Fig. 3, an edge $e_{ij} = s_i s_j$ can be used for building one triangle on each of its two sides. Suppose the formed triangle is $\triangle s_i s_j s_k$. When two nodes are connected by a new edge (e.g., $s_i s_k$ and $s_j s_k$), if the new edge is a potential edge, the edged nodes conduct the same operation by choosing their NTN to construct a new triangle with the minimum circumcircle.

Each node stores the triangles it belongs to in its Delaunay triangulation table (DT-table). This process continues until a newly added edge intersects with an existing edge, which means the triangulation is completed. However, it is difficult to globally notify all nodes of completion. Also, a node isolated from the others may keep looking for nodes to build triangle edges. Thus, DECM sets an appropriate time period for each node to conduct the triangulation process. After the time period, each node checks to see if an *illegal edge* exists in the triangles in its DT-Table, and conducts an *edge flip* if an *illegal edge* exists. This step is to ensure that Delaunay triangulation is formed according to *Theorem 3.2*. There should not be many *illegal edges* because:

Theorem 3.3: When two edged nodes connect to their NTN to construct a triangle, there are no other nodes inside the triangle's circumcircle on the same side as the NTN.

Proof: As Fig. 5 (a) and (b) show, s_k is the NTN of e_{ij}, and s_i, s_j, and s_k construct a triangle (either acute or obtuse), in which $O_{k,ij}$ is the circumcenter of the triangle. Suppose there is one sensor node $s_{k'}$ located inside the triangle on the same side of e_{ij} as s_k (i.e., $s_{k'}O_{k,ij} < s_j O_{k',ij}$). The perpendicular bisector of $s_i s_{k'}$ definitely intersects $s_i O_{k,ij}$ and $M_{ij}O_{k,ij}$ at point $O_{k',ij}$. Therefore, $h_{k',ij} = h_{k,ij} - O_{k,ij}O_{k',ij}$, which indicates that $h_{k,ij} \leq h_{k',ij}$. This contradicts the definition of the NTN. ■

Note that two edged nodes are not necessarily neighbors. Nodes can communicate with each other by multi-hop routing [24]. Though two edged nodes calculate their NTN individually, they will find the same NTN result when their r-maps include their nearby nodes. Also, because only one NTN exists on one side of a potential edge of two edged nodes, it is impossible that a new edge will intersect with an existing edge of the two nodes.

The Delaunay triangulation can take $O\left(n^2\right)$ (n is the number of nodes in the network) edge flips even if all node locations are globally known [22]. A local edge flip might generate new illegal triangles, and then the computation might be endless, though the probability of such an event is low according to Theorem 3.3. To avoid endless edge flipping, we set a Time To Live (TTL) for each sensor node. Once the TTL expires, a node stops flipping edges even though it finds illegal triangles. The TTL strategy does not prevent DECM from achieving full coverage but might generate unnecessary node movements. The strategy might reduce the accuracy of Delaunay triangulation since there could exist some illegal triangles. That is, some other node besides the triangle's three nodes could cover the circumcircle's center. Then, the coverage holes that the three sensor nodes have detected might be covered by some other nodes, leading to unnecessary node movements. In this paper, we assume that the node density is high enough for Delaunay triangulation and that the number of node movement iterations for hole healing is limited.

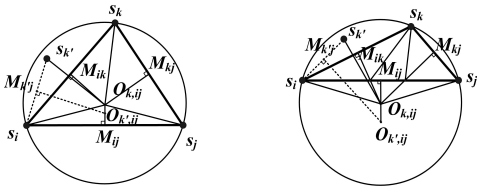

(a) Acute triangle (b) Obtuse triangle

Figure 5. Proof of *Theorem 3.3*.

Specifically, in conducting Delaunay triangulation on a WSN, each node s_i executes Algorithm 1.

Algorithm 1 The algorithm for Delaunay triangulation executed by s_i.

Step 1: If it is selected as the seed node, go to Step 2; otherwise, go to Step 3.
Step 2: Find the nearest node in its r-map, say s_j, and build an edge to s_j. Store edge e_{ij} into its DT-table and also ask s_j to store e_{ij} into its DT-table.
Step 3: Check if its DT-table contains *potential edges*. If yes, find the NTN of each *potential edge* and build an edge to the NTN; otherwise, go to Step 4.
Step 4: Check whether the time is expired. If no, go to step 3; otherwise go to Step 5.
Step 5: In TTL, flip edge for each existing *illegal edge*.

C. Safe Area Detection

Definition 8 (*safe area*): Consider a triangle formed by three nodes s_i, s_j, and s_k, where s_i and s_j are not moving. The *safe area* of s_k for $\triangle s_i s_j s_k$ is defined as the area where s_k can be located without breaking the full coverage of $\triangle s_i s_j s_k$.

In the following, we calculate s_k's *safe area*. We assume that s_i's r-map contains s_j and s_k and use s_i's r-map for the calculation. Using the r-maps of s_j or s_k can retrieve the same results. First, we assume that $\theta_{ik} \in [\theta_{ij},\ \theta_{ij} + \pi)$. We will discuss the situation when $\theta_{ik} \in [0,\ \theta_{ij}) \cup [\theta_{ij} + \pi,\ 2\pi)$ later on. There are three different kinds of triangle shapes for $\triangle s_i s_j s_k$:
Case I: an acute triangle (Fig. 6 (a));

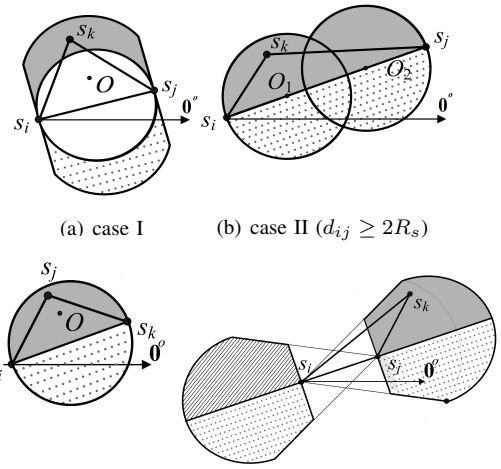

(a) case I (b) case II ($d_{ij} \geq 2R_s$)

(c) case II ($d_{ij} < 2R_s$) (d) case III

Figure 6. Node s_k's *safe area*.

Case II: an obtuse triangle with $d_{ij} > max\{d_{ik},\ d_{jk}\}$ (Fig. 6 (b) and (c));
Case III: an obtuse triangle with $d_{ij} < max\{d_{ik},\ d_{jk}\}$ (Fig. 6 (d)).

Case I When $\triangle s_i s_j s_k$ is an acute triangle: As Fig. 6 (a) shows, d_{ij}, d_{jk}, and d_{ik} must satisfy $d_{ij}^2 + d_{ik}^2 > d_{jk}^2$, $d_{ij}^2 + d_{jk}^2 > d_{ik}^2$, and $d_{ik}^2 + d_{jk}^2 > d_{ij}^2$, which can be induced to:

$$d_{ij} - d_{ik}\cos(\theta_{ik} - \theta_{ij}) > 0 \ \ and \ \ \theta_{ij} < \theta_{ik} < \theta_{ij} + \frac{\pi}{2} \quad (4)$$

To guarantee the full coverage of the triangle, Eq. (1) in *Theorem 3.1* must be satisfied, which can be simplified to:

$$\left(\frac{d_{ik}\cos\theta'_{ik}\left(d_{ij} - d_{ik}\cos\theta'_{ik}\right)}{d_{ik}\sin\theta'_{ik}} - d_{ik}\sin\theta'_{ik}\right)^2 + d_{ij}^2 \leq 4R_s^2 \quad (5)$$

where $\theta'_{ik} = \theta_{ik} - \theta_{ij}$. From Eq. (5), we can derive $d_{ij} < 2R_s$ and

$$\left(d_{ik}\cos\theta'_{ik} - \frac{d_{ij}}{2}\right)^2 + \left(d_{ik}\sin\theta'_{ik} + \frac{\sqrt{4R_s^2 - d_{ij}^2}}{2}\right)^2 \geq R_s^2 \quad (6)$$

$$\left(d_{ik}\cos\theta'_{ik} - \frac{d_{ij}}{2}\right)^2 + \left(d_{ik}\sin\theta'_{ik} - \frac{\sqrt{4R_s^2 - d_{ij}^2}}{2}\right)^2 \leq R_s^2 \quad (7)$$

where $\theta'_{ik} = \theta_{ik} - \theta_{ij}$. Therefore,

Lemma 3.1: $d_{ij} < 2R_s$ is a necessary condition for the full coverage of an acute triangle (Case I). The area formed by Eq. (4), Eq. (6), and Eq. (7) is the *safe area* of s_k, which is the gray area in Fig. 6 (a).

Case II When $\triangle s_i s_j s_k$ is an obtuse triangle with $d_{ij} > max\{d_{ik},\ d_{jk}\}$: As Fig. 6 (b) shows, d_{ij}, d_{jk}, and d_{ik} must satisfy $d_{ij}^2 \geq d_{jk}^2 + d_{ik}^2$, which can be simplified to:

$$d_{ik} \leq d_{ij}\cos(\theta_{ik} - \theta_{ij}) \quad (8)$$

To guarantee full coverage of the triangle, Eq. (2) in *Theorem 3.1* must be satisfied. We discuss the problem in two cases:

Case II.1 When $d_{ik} \geq d_{jk}$, Eq. (2) can be induced to:

$$\frac{d_{ik}}{\cos(\theta_{ik} - \theta_{ij})} \leq 2R_s. \quad (9)$$

The area formed by Eqs. (8) and (9) is the safe area *of s_k, which is the gray area in Fig. 6 (b).*

We notice that when $d_{ij} < 2R_s$, if Eq. (8) is satisfied, Eq. (9) is automatically satisfied, indicating that the triangle is fully covered. This is because:

$$\frac{d_{ik}}{\cos(\theta_{ik} - \theta_{ij})} \leq d_{ij} < 2R_s \ \rightarrow \ \frac{d_{ik}}{\cos(\theta_{ik} - \theta_{ij})} \leq 2R_s \quad (10)$$

Case II.2 When $d_{ik} < d_{jk}$, Eq. (2) can be reduced to:

$$\frac{d_{ik}^2 - 2d_{ik}d_{ij}\cos(\theta_{ik} - \theta_{ij}) + d_{ij}^2}{d_{ij} - d_{ik}\cos(\theta_{ik} - \theta_{ij})} \leq 2R_s \quad (11)$$

Similarly, we notice that when $d_{ij} < 2R_s$, if Eq. (8) is satisfied, Eq. (11) is automatically satisfied, indicating that the triangle is fully covered. This is because Eq. (8) can be reduced to

$$d_{ik}^2 - 2d_{ik}\cos\theta'_{ik}d_{ij} + d_{ij}^2 \leq d_{ij}^2 - d_{ik}\cos\theta'_{ik}d_{ij}, \quad (12)$$

where θ'_{ik}=θ_{ik}−θ_{ij}. Because $d_{ij} - d_{ik}\cos(\theta_{ik} - \theta_{ij}) > 0$ in Eq. (8), Eq. (12) can be reduced to

$$\frac{d_{ik}^2 - 2d_{ik}\cos(\theta_{ik} - \theta_{ij})d_{ij} + d_{ij}^2}{d_{ij} - d_{ik}\cos(\theta_{ik} - \theta_{ij})} < d_{ij} < 2R_s \quad (13)$$

Thus, Eq. (11) is satisfied. Accordingly,

Lemma 3.2: For an obtuse triangle with $d_{ij} > max\{d_{ik},\ d_{jk}\}$ (Case II), when $d_{ij} < 2R_s$, Eq. (8) is a sufficient condition for the full coverage of the triangle, and the area formed by Eq. (8) is the *safe area* of s_k, which is the gray area in Fig. 6 (c); when $d_{ij} \geq 2R_s$, the area formed by Eq. (8), Eq. (9), and Eq. (11) is the *safe area* of s_k, which is the gray area in Fig. 6 (b).

Case III When $\triangle s_i s_j s_k$ is an obtuse triangle with $d_{ij} < max\{d_{ik},\ d_{jk}\}$: This case is further discussed in the following two cases:

Case III.1 When $d_{ik} > max\{d_{ij},\ d_{jk}\}$: As Fig. 6 (d) shows, d_{ij}, d_{jk}, and d_{ik} must satisfy $d_{ik}^2 > d_{ij}^2 + d_{jk}^2$, which can be reduced to:

$$d_{ik}\cos(\theta_{ik} - \theta_{ij}) > d_{ij} \quad (14)$$

where $\cos(\theta_{ik} - \theta_{ij}) > 0$ because $d_{ik} > d_{jk}$. To guarantee full coverage of the triangle, Eq. (2) in *Theorem 3.1* should be satisfied. We discuss the problem in two cases:

Case III.1.1 When $d_{ik} > d_{ij} \geq d_{jk}$: From Equ. (2), the *safe area* of s_k can be calculated as:

$$\frac{d_{ij}}{2\cos(\theta_{ik} - \theta_{ij})} \leq R_s \text{ and } \frac{d_{ik}}{2\cos(\theta_{ik} - \theta_{ij})} < d_{ij} \quad (15)$$

From Eqs. (14) and (15), we can infer that:

$$\frac{d_{ij}}{2R_s} \leq \cos(\theta_{ik} - \theta_{ij}) < 1 \rightarrow d_{ij} < 2R_s \quad (16)$$

Case III.1.2 When $d_{ik} > d_{jk} > d_{ij}$: From Eq. (2), the *safe area* of s_k can be calculated as:

$$\frac{d_{ik}^2 - 2d_{ik}d_{ij}\cos(\theta_{ik} - \theta_{ij}) + d_{ij}^2}{2(d_{ik} - d_{ij}\cos(\theta_{ik} - \theta_{ij}))} \leq R_s \quad (17)$$

$$\frac{d_{ik}}{2\cos(\theta_{ik} - \theta_{ij})} > d_{ij} \quad (18)$$

Recall that $d_{ij} < 2R_s$ when $d_{ij} > d_{jk}$. Similarly, we can derive that $d_{jk} < 2R_s$ when $d_{jk} > d_{ij}$. Then,

$$d_{ij} < d_{jk} < 2R_s \rightarrow d_{ij} < 2R_s \tag{19}$$

From Eqs. (16) and (19), we know that

Lemma 3.3: $d_{ij} < 2R_s$ is a necessary condition for the full coverage of an obtuse triangle with $d_{ik} > max\{d_{ij}, d_{jk}\}$ (Case III). The area formed by Eq. (14), Eq. (15), and Eq. (17) is the *safe area* of s_k, which is the gray area in Fig. 6 (c).

Case III.2 When $d_{jk} \geq max\{d_{ij},\ d_{ik}\}$: If we use s_j's r-map to calculate s_k's *safe area* in the obtuse triangle, because this is symmetrical to Case III.1, the calculated s_k's *safe area* is similar to that of case III.1 shown in the slashed area of Fig. 6 (d). In other cases, using s_j's r-map to calculate s_k's *safe area* leads to exactly the same result. When $\theta_{ik} \in [0,\ \theta_{ij}) \cup [\theta_{ij} + \pi,\ 2\pi)$, it only results in a safe area that is symmetrical to the area when $\theta_{ik} \in [\theta_{ij},\ \theta_{ij} + \pi)$ as shown in the dotted and gray areas in Fig. 6 (a)-(d).

From Lemmas 3.1, 3.2, and 3.3, we know that when s_i looks for the safe area of s_k for full coverage of $\triangle s_i s_j s_k$, given d_{ij}, if $d_{ij} \geq 2R_s$, s_k's safe area is only Fig. 6(b) in Case II, which is re-drawn in Fig. 7 (b). If $d_{ij} < 2R_s$, s_k's safe area can be Fig. 6 (a), (c), and (d) in Case I, II, and III, the combination of which is shown in Fig. 7 (b).

Theorem 3.4: When s_i checks the full coverage of $\triangle s_i s_j s_k$, given d_{ij} when $d_{ij} \geq 2R_s$, the gray area in Fig. 7(b) is the safe area of s_k; otherwise, the gray area in Fig. 7(a) is the safe area of s_k.

If every node only has the relative location information of other nodes, it would be difficult for the system to detect holes on the edge of the target region [20]. There are several ways to solve this problem, such as configuring nodes before placing them. In our system, we deploy a small number of static nodes on the edge of the region as *anchor nodes* to help detect holes.

D. Shortest-path Movement

Recall that after the Delaunay triangulation, each node stores the nodes that are in the same triangle as itself in its *DT-Table*. We call these nodes *triangle neighbors* of the node. Each node calculates the safe areas of its triangle neighbors, checks to see if they are in their own safe areas using its r-map based on Theorem 3.4, and then notifies those which are not in their own safe areas. After a node receives an out-of-safe-area notification, it calculates the target point that leads to the shortest path in order to cover the hole. A node may receive multiple out-of-safe-area notifications, similar to VOR [7]; the node then moves to the farthest target point in order to fix the largest hole, so that the sizes of all holes in the WSN are quickly reduced. Differently from VOR, in which a node movement may lead to numerous iterations to cover a hole, DECM enables a node to move to its destination directly to cover a hole and meanwhile keep the full coverage of its triangle. In the following, we present the algorithm to calculate the shortest path for node movement.

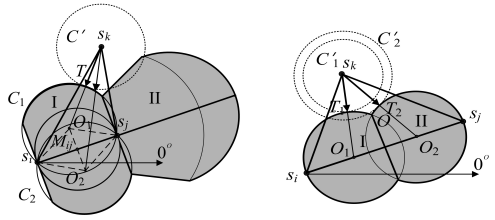

(a) when $d_{ij} < 2R_s$ (b) when $d_{ij} \geq 2R_s$

Figure 7. Shortest path in node movement for hole healing.

Assume that s_k receives the notification from s_i along with d_{ij} and s_k's *safe area*. s_k then calculates its shortest path and the target point to move into its *safe area*. Similar to hole detection, s_k needs to consider two cases according to d_{ij}.

Case I When $d_{ij} < 2R_s$: As Fig. 7 (a) shows, the *safe area* for s_k is composed of two parts: area I and area II. From Eq. (7) we can get the polar coordinates of C_1's center O_1 and C_2's center O_2: $(R_s,\ \arccos\left(\frac{s_{ij}}{2R_s}\right) + \theta_{ij})$ and $(R_s,\ 2\pi - \arccos\left(\frac{s_{ij}}{2R_s}\right) - \theta_{ij})$. s_k has two choices: (1) constructing an acute triangle (moving towards area I), and (2) constructing an obtuse triangle (moving towards area II). We only let nodes contruct acute triangles because this makes the node positions more similar to the vertices of the static hexagon based permutation, which is considered the best for node distribution [25]. To find the shortest path and target point to move to region I, using itself as the circle center, s_k draws a circle C', which generates a point of tangent between C' and region I, denoted T; then s_kT is the shortest path. T is on the line of s_kO_1 if $\theta_{ik} \in [\theta_{ij},\ \theta_{ij} + \pi)$ and is on the line of s_kO_2 if $\theta_{ik} \in [0,\ \theta_{ij}) \cup [\theta_{ij} + \pi,\ 2\pi)$. Thus, to cover the hole, s_k moves towards point O_1 or O_2, whichever is nearer, and stops once it enters its safe area. As a result, it moves along the shortest path, the length of which is:

$$s_kT = \sqrt{\left(x_{ik} - \frac{d_{ij}}{2}\right)^2 + \left(y_{ik} - \frac{\sqrt{4R_s^2 - d_{ij}^2}}{2}\right)^2} - R_s \tag{20}$$

where $x_{ik} = d_{ik}\cos(\theta_{ik} - \theta_{ij})$, $y_{ik} = d_{ik}\sin(\theta_{ik} - \theta_{ij})$.

Node s_k can independently calculate the coordinates of O_1 and O_2 in its own r-map. We notice that the polar coordinates of point O_1 and O_2 must be positioned at s_i and s_j's perpendicular bisector and that $O_1s_i = O_2s_i = R_s$. Accordingly, the coordinates of O_1 in s_k's r-map, $(d_{kO_1}, \theta_{kO_1})$, can be calculated by:

$$d_{kO_1} = \sqrt{(A+B)^2 + (C+D)^2} \tag{21}$$

$$\theta_{kO_1} = \begin{cases} \arctan\left(\frac{C+D}{A+B}\right) & \text{if } C+D \geq 0 \\ \arctan\left(\frac{C+D}{A+B}\right) + \pi & \text{if } C+D < 0 \end{cases} \tag{22}$$

The coordinates of O_2 in s_k's r-map, $(d_{kO_2}, \theta_{kO_2})$, can be calculated by:

$$d_{kO_2} = \sqrt{(A-B)^2 + (C-D)^2} \tag{23}$$

$$\theta_{kO_1} = \begin{cases} \arctan\left(\frac{C-D}{A-B}\right) & \text{if } C-D \geq 0 \\ \arctan\left(\frac{C-D}{A-B}\right) + \pi & \text{if } C-D < 0 \end{cases} \quad (24)$$

where

$$A = \frac{d_{ki}\cos\theta_{ki} + d_{kj}\cos\theta_{kj}}{2},\ C = \frac{d_{ki}\sin\theta_{ki} + d_{kj}\sin\theta_{kj}}{2}$$

$$B = \frac{\sqrt{R_s^2 - \left(\frac{d}{2}\right)^2}\left(d_{kj}\sin\theta_{kj} - d_{ki}\sin\theta_{ki}\right)}{d}$$

$$D = \frac{\sqrt{R_s^2 - \left(\frac{d}{2}\right)^2}\left(d_{ki}\cos\theta_{ki} - d_{kj}\cos\theta_{kj}\right)}{d}$$

$$\text{and } d = \sqrt{d_{ki}^2 - 2\cos\left(\theta_{ki} - \theta_{kj}\right)d_{ki}d_{kj} + d_{kj}^2}$$

Based on the coordinates of O_1 and O_2, s_k chooses the one closer to itself as the target point, which leads to the shortest moving path.

Case II When $d_{ij} \geq 2R_s$: As Fig. 7 (b) shows, the polar coordinate of O_1 and O_2 in s_k's r-map are (R_s, θ_{ij}) and $(d_{ij} - R_s, \theta_{ij})$, respectively. s_k also has two choices: (1) moving towards region I, and (2) moving towards region II. Node s_k chooses the option that leads to the shorter moving path. Specifically, s_k produces the circle C_1', which has s_k as its center and has a tangent with region I at point T_1. s_k also produces the circle C_2', which has s_k as its center and has a tangent with region II at point T_2.

If $T_1 s_k < T_2 s_k$, the direction of s_k's movement is towards O_1 and the length of the shortest path $T_1 s_k$ is:

$$T_1 s_k = \sqrt{d_{ik}^2 - d_{ik}d_{ij}\cos l\left(\theta_{ik} - \theta_{ij}\right) + \frac{d_{ij}^2}{4}} - R_s \quad (25)$$

If $T_1 s_k \geq T_2 s_k$, the direction of s_k's movement is towards O_2 and the length of the shortest path $T_2 s_k$ is:

$$T_2 s_k = \sqrt{d_{ik}^2 - 2d_{ik}\cos\theta'_{ik}\left(R_s - \frac{d_{ij}}{2}\right) + \left(R_s - \frac{d_{ij}}{2}\right)^2} - R_s \quad (26)$$

where $\theta'_{ik} = \theta_{ik} - \theta_{ij}$. Similar to Case I, in Case II s_k can figure out the coordinates of O_1 and O_2 through its own r-map's information. Both O_1 and O_2 are located at $s_i s_j$, and $O_1 s_i = O_2 s_j = R_s$. The coordinates of O_1 in s_k's r-map, $(d_{kO_1}, \theta_{kO_1})$, can be calculated by:

$$d_{kO_1} = \sqrt{A^2 + B^2} \quad (27)$$

$$\theta_{kO_1} = \begin{cases} \arctan\left(\frac{B}{A}\right) & \text{if } B \geq 0 \\ \arctan\left(\frac{B}{A}\right) + \pi & \text{if } B < 0 \end{cases} \quad (28)$$

The coordinate of O_2 in s_i's r-map, $(d_{kO_2}, \theta_{kO_2})$, can be calculated by:

$$d_{kO_2} = \sqrt{C^2 + D^2} \quad (29)$$

$$\theta_{kO_2} = \begin{cases} \arctan\left(\frac{D}{C}\right) & \text{if } D \geq 0 \\ \arctan\left(\frac{D}{C}\right) + \pi & \text{if } D < 0 \end{cases} \quad (30)$$

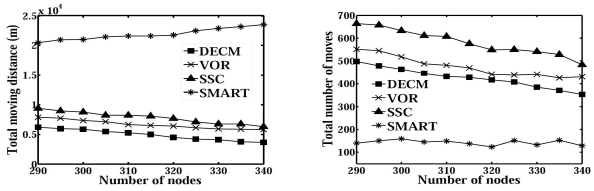

(a) Total moving distance (b) Total number of moves

Figure 8. Energy-efficiency of different schemes with different number of nodes (simulation).

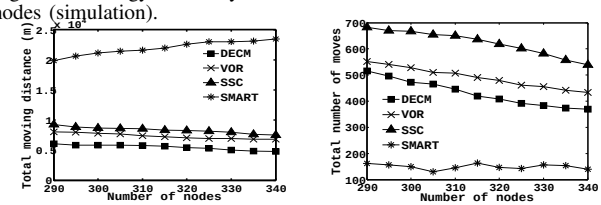

(a) Total moving distance (b) Total number of moves

Figure 9. Energy-efficiency of different schemes with different number of nodes (Orbit Testbed).

where

$$A = d_{ki}\cos\theta_{ki} + \frac{R_s\left(d_{kj}\cos\theta_{kj} - d_{ki}\cos\theta_{ki}\right)}{d} \quad (31)$$

$$B = d_{ki}\sin\theta_{ki} + \frac{R_s\left(d_{kj}\sin\theta_{kj} - d_{ki}\sin\theta_{ki}\right)}{d} \quad (32)$$

$$C = d_{kj}\cos\theta_{kj} - \frac{R_s\left(d_{kj}\cos\theta_{kj} - d_{kj}\cos\theta_{kj}\right)}{d} \quad (33)$$

$$D = d_{kj}\sin\theta_{kj} - \frac{R_s\left(d_{kj}\sin\theta_{kj} - d_{ki}\sin\theta_{ki}\right)}{d} \quad (34)$$

$$\text{and } d = \sqrt{d_{ki}^2 - 2\cos\left(\theta_{ki} - \theta_{kj}\right)d_{ki}d_{kj} + d_{kj}^2}.$$

Based on the coordinates of O_1 and O_2, s_k moves towards the point closest to it, which leads to the shortest moving path.

IV. Performance Evaluation

In this section, we present the experimental results from the simulation and the experiments on GENI Orbit testbed [26], [27]. The testbed uses a large two-dimensional grid of 400 802.11 radio nodes, which can be dynamically interconnected into specified topologies. We compared DECM with other three movement schemes for WSN full coverage: VORonoi-based algorithm (VOR) [7], Scan-based Movement-Assisted Sensor Deployment (SMART) [5] and Sea Surface Coverage (SSC) [15]. In SSC, nearby nodes can only move in four directions to inherit others' lost "interest points". Since the target region is not fully covered at the beginning in our simulation environment, we assume that every "interest point" in SSC is assigned to its nearest node. We also compared DECM with DECM-R, in which each node randomly selects one target point from multiple notifications, and with DECM-S, in which each node selects the nearest target point from multiple notifications. The nodes in Orbit do not move. We simulated the node movement by letting nodes exchange the information of their virtual locations.

The target field is a $1200m \times 1200m$ area. The number of sensors was varied from 290 to 340. The radius of the sensing range was varied from 55.2m to 59.2m and the

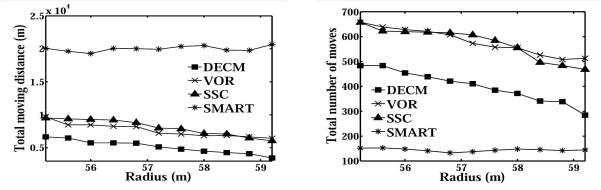

(a) Total moving distance (b) Total number of moves

Figure 10. Energy-efficiency of different schemes with different radii (simulation).

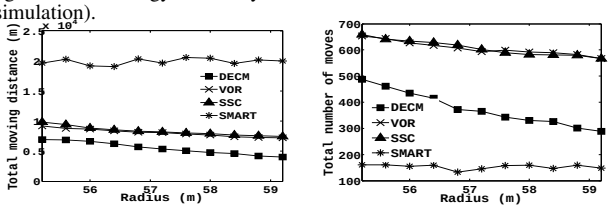

(a) Total moving distance (b) Total number of moves

Figure 11. Energy-efficiency of different schemes with different radii (Orbit Testbed).

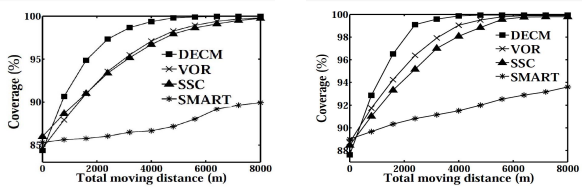

(a) The number of nodes is 300 (b) The number of nodes is 330

Figure 12. Efficiency of healing holes in different schemes (simulation).

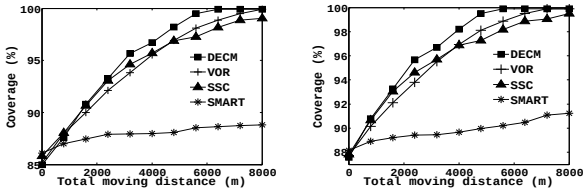

(a) The number of nodes is 300 (b) The number of nodes is 330

Figure 13. Efficiency of healing holes in different schemes (Orbit Testbed).

transmission range was set to 120m. Initially, we randomly distributed all sensors in the target field. Then we used a scheme to heal the holes until the coverage reaches 99.9%. We measured the following metrics.

(1) *Total moving distance.* This is the sum of the moving distances of all nodes for hole healing. It reflects the delay and energy cost of node movement in hole healing. As in the work in [15], we do not consider the energy consumption for node communication and computing, because it is much lower than that of physical movement.

(2) *Total number of moves.* This is the sum of the number of moves of all nodes for hole healing. Since node moving startup usually consumes more energy than moving, this metric also reflects the energy consumption.

(3) *Coverage.* We distribute 10,000 points uniformly throughout the entire field. The coverage equals the percent points covered. This metric represents the effectiveness of full coverage schemes.

A. Energy Cost of Healing Holes

Fig. 8 and Fig. 9 show the *total moving distance* and *total number of moves* versus the number of nodes in different schemes in simulation and Orbit testbed, respectively. From these figures, we find that DECM has the best performance in *total moving distance*. The *total moving distance* follows SMART$\gg$ SSC $>$ VOR $>$ DECM, and the *total number of moves* follows SSC$>$ VOR $>$ DECM $\gg$ SMART in both simulation and Orbit.

Both SSC and VOR have higher costs in both metrics than DECM because they cannot find the shortest paths for node movement to heal the holes. Long moving paths may produce new holes because a node may not be able to cover its original area after moving, thus resulting in more movements. In DECM, each triangle is managed by three nodes. A node's movement aims to fully cover its triangle. Even when a node selects its farthest target point when receiving multiple notifications, a potential new hole in the triangle can be healed by the other two sensor nodes. In VOR, each Voronoi cell is managed by only one node. A node's movement aims to cover one point in its cell, which makes it very likely to generate new holes within its Voronoi cell that cannot be managed by any other nodes. As a result, this node may move back, or other nodes may need to move to cover the hole, resulting in more iterations of node movement. Thus, VOR produces a longer total moving distance and a greater total number of moves than DECM.

It is very intriguing to see that SMART generates a significantly higher total moving distance than the others while producing the lowest total number of moves. Recall that the main task of SMART is to balance the distribution of sensor nodes throughout the entire target region in order to achieve full coverage. Even when the region has no hole, nodes need to make movements to achieve balance. Since the decision of node movement is made by cluster heads, each of which holds all the information of nodes in its cluster, there is only one iteration and every node only needs one movement to reach its final target point. Consequently, SMART generates a long total moving path but a low number of moves.

Fig. 10 and Fig. 11 show the *total moving distance* and *total number of moves* versus the node sensing radius in different schemes in simulation and Orbit testbed, respectively. We see that the *total moving distance* follows SMART $\gg$ VOR $\approx$ SSC $>$ DECM, and the *total number of moves* follows VOR $\approx$ SSC$>$DECM$\gg$SMART in both simulation and Orbit. This is for the same reasons as in Fig. 8. We also observe that for DECM, VOR, and SSC, the two metric results decrease as the radius of sensing range increases. This is because a larger sensing range can reduce the number and size of coverage holes. SMART is not affected significantly by the change of sensing radius because it aims to balance the sensor distribution.

B. Effectiveness of Healing Holes

Fig. 11 and Fig. 12 show that the *coverage* versus the *total moving distance* in different schemes in simulation and Orbit testbed, respectively. Fig. 11 (a) and Fig. 12 (a) show that to achieve 99.9% coverage, the total moving distance is 5600m in DECM, but is over 8000m in other schemes. Fig. 11 (b) and Fig. 12 (b) show that to achieve 99.9% coverage, the total moving distance is 4000m in

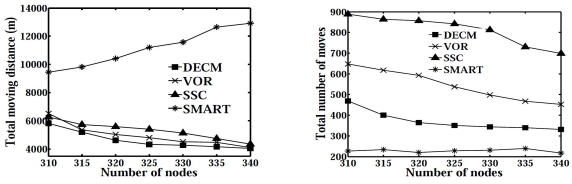

(a) Total moving distance (b) Total number of moves

Figure 14. Energy-efficiency of different schemes in handling dead nodes (simulation).

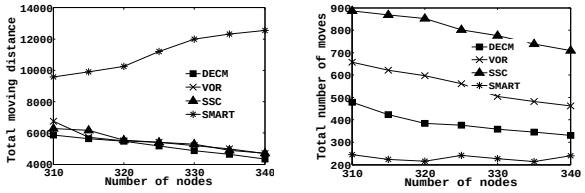

(a) Total moving distance (b) Total number of moves

Figure 15. Energy-efficiency of different schemes in handling dead nodes (Orbit Testbed).

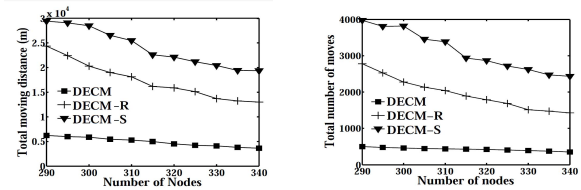

(a) Total moving distance (b) Total number of moves

Figure 16. Energy-efficiency of DECM with different target point selections (simulation).

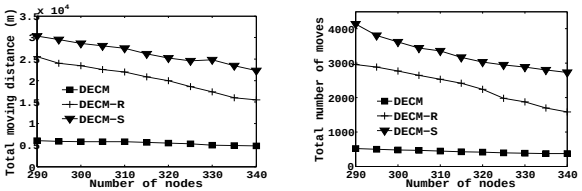

(a) Total moving distance (b) Total number of moves

Figure 17. Energy-efficiency of DECM with different target point selections (Orbit Testbed).

DECM, is 5600m in VOR, and is over 8000m in SSC and SMART. DECM always finds the shortest paths for healing holes. A shorter movement distance has a lower probability of generating new holes. Also, three nodes managing a triangle area rather than one node makes it easier to heal newly generated holes caused by a node's movement. More importantly, a node's movement covers the entire triangle rather than a point. Thus, DECM avoids excessive iterations of node movement and achieves full coverage more rapidly than other schemes. The figures show that SMART achieves full coverage very slowly. This is because the objective of SMART is to balance the distribution of nodes and thus hole sizes are not decreased rapidly. Comparing (a) and (b) in Fig. 12 and Fig. 12, we see that more sensors help achieve full coverage faster in all schemes because a higher node density reduces the number and size of holes.

C. Healing Holes Due to Dead Nodes

In this experiment, 50 nodes died immediately after all holes were healed from the initial deployment. Fig. 14 (a) and (b), and Fig. 15 (a) and (b) show the *total moving distance* and *number of moves* of the schemes in healing the holes caused by the dead nodes in simulation and Orbit testbed, respectively. We see that the *total moving distance* follows SMART$\gg$SSC$>$VOR$>$DECM, and that the *total number of moves* follows SSC$>$VOR$>$DECM$>$SMART in both simulation and Orbit. This is for the same reasons as in Fig. 8. The results show that DECM still exhibits superior performance over others even with dead nodes.

D. Different Target Point Selections

Fig. 16 and Fig. 17 show the *total moving distance* and *total number of moves* of DECM, DECM-R and DECM-S in different schemes in simulation and Orbit testbed, respectively. We see that DECM generates significantly lower results in both metrics than DECM-R and DECM-S. The results verify the effectiveness of DECM in choosing the farthest target point. It can quickly reduce the sizes of large holes, and hence reduce the number of moves. Also, moving towards large holes can balance the distribution of nodes over the entire target region more quickly. From our observations, when nodes move to heal small-size holes, new holes may arise in the original position. Then, the node will move back to heal the newly generated small holes, leading to more iterations.

Fig. 18 and Fig. 19 show the *coverage* versus the *total moving distance* in DECM, DECM-R, and DECM-S when the number of sensors is set to 300 and 330, in simulation and Orbit testbed, respectively. In both figures, DECM achieves full coverage more rapidly than DECM-R and DECM-S. In Fig. 18 (a) and Fig. 19 (a), when the *total moving distance* reaches 5600m, DECM achieves 99.9% coverage, while DECM-R and DECM-S achieve 98.12% and 96.01% coverage, respectively. In Fig. 18 (b) and Fig. 19 (b), when the *total moving distance* reaches 4800m, DECM achieves 99.9% coverage, while DECM-R and DECM-S only achieve 98.27% and 96.89% coverage, respectively. Because DECM always fixes the largest hole first since it selects the farthest target point, it reduces the size of holes more and achieves the full coverage faster than DECM-R and DECM-S.

From the experimental results, we find that there is no big difference between the simulation results and Orbit real-world testbed results. It is because in the Orbit testbed, we used virtual location exchanges between static nodes to simulate node movement and there is no packet loss during the testing process. The experimental results verify that selecting the farthest target point when finding several uncovered triangles is the optimal method in healing holes. In summary, the simulation and real testbed results show:

1) DECM is more energy-efficient for full coverage than other schemes, even when some sensor nodes die.

2) DECM can heal coverage holes more quickly than other schemes.

3) Selecting the farthest target point when finding several

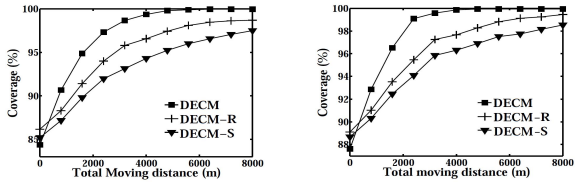

(a) The number of nodes is 300 (b) The number of nodes is 330

Figure 18. Effectiveness of healing holes in DECM with different target point selections (simulation).

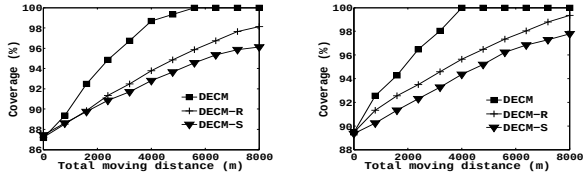

(a) The number of nodes is 300 (b) The number of nodes is 330

Figure 19. Effectiveness of healing holes in DECM with different target point selections (Orbit Testbed).

triangles that are not fully covered is an optimal method in DECM.

ACKNOWLEDGEMENTS

This research was supported in part by U.S. NSF grants OCI-1064230, CNS-1049947, CNS-1156875, CNS-0917056 and CNS-1057530, CNS-1025652, CNS-0938189, CSR-2008826, CSR-2008827, Microsoft Research Faculty Fellowship 8300751, and Oak Ridge Award 4000111689.

The authors are grateful to Dr. Xiangyang Li for his helpful comments on this paper.

REFERENCES

[1] S. Chellappan, W. Gu, X. Bai, D. Xuan, and K. Zhang, "Deploying wireless sensor networks under limited mobility constraints," in *IEEE TMC*, 2007.

[2] S. Chellappan, X. Bai, B. Ma, D. Xuan, and C. Xu, "Mobility limited flip-based sensor networks deployment," in *IEEE TPDS*, 2007.

[3] Z. Jiang, J. Wu, R. Kline, and J. Krantz, "Mobility control for complete coverage in wireless sensor networks," in *Proc. of ICDCSW*, 2008.

[4] G. Wang, G. Cao, T. F. L. Porta, and W. Zhang, "Sensor relocation in mobile sensor networks," in *Proc. of INFOCOM*, 2005.

[5] S. Yang, M. Li, and J. Wu, "Scan-based movement-assisted sensor deployment methods in wireless sensor networks," in *IEEE TPDS*, 2007.

[6] Y. Zou and K. Chakrabarty, "Energy-aware target localization in wireless sensor networks," in *Proc. of PerCom*, 2003.

[7] G. Wang, G. Cao, and T. F. L. Porta, "Movement-assisted sensor deployment," in *Proc. of INFOCOM*, 2004.

[8] Y. Zou and K. Chakrabarty, "Sensor deployment and target localization based on virtual forces," in *Proc. of INFOCOM*, 2003.

[9] K. Akkaya and S. Janapala, "Maximizing connected coverage via controlled actor relocation in wireless sensor and actor networks," in *Computer Networks*, 2008.

[10] N. Heo and P. Varshney, "Energy-efficient deployment of intelligent mobile sensor networks.," in *ITSMC*, 2005.

[11] Z. Butler and D. Rus, "Event-based motion control for mobile sensor networks," in *Pervasive Computing*, 2003.

[12] H. Zhang and A. Arora, "Gs3: Scalable self-configuration and self-healing in wireless networks," in *Computer Networks*, 2003.

[13] N. Heo and P. K. Varshney, "An intelligent deployment and clustering algorithm for a distributed mobile sensor network," in *ITSMC*, 2003.

[14] W. Heinzelman, A. Chandrakasan, and H. Balakrishnan, "Energyefficient communication protocol for wireless microsensor networks," in *Proc. of HICSS*, 2000.

[15] J. Luo, D. Wang, and Q. Zhang, "Double mobility: Coverage of the sea surface with mobile sensor networks.," in *Proc. of INFOCOM*, 2009.

[16] L. Xu and D. Evans, "Localization for mobile sensor networks," in *Proc. of MobiCom*, 2004.

[17] D. R. D. Moore, J. Leonard and S. Tell, "Robust distributed network localization with nosiy range measurements," in *Proc. of SenSys*, 2004.

[18] S. Lee, Z.-L. Zhang, S. Sahu, and D. Saha, "On suitability of euclidean embedding of internet hosts," in *SIGMETRICS*, 2006.

[19] D. Niculescu, "Positioning in ad hoc sensor networks," in *IEEE Network Volume*, 2004.

[20] Y. Bejerano, Bell-Labs, Alcatel-Lucent, M. Hill, and N.J., "Simple and efficient k-coverage verification without location information," in *Proc. of INFOCOM*, 2008.

[21] Y. Xu, J. Heidemann, and D. Estrin, "Geographyinformed energy conservation for ad hoc routing," in *Proc. of MobiCom*, 2001.

[22] M. de Berg, O. Cheong, M. van Kreveld, and M. Overmars, "Computational geometry: Algorithm and applications," *Springer*, 2008.

[23] G. S. Kasbekar, Y. Bejerano, and S. Sarkar, "Lifetime and coverage guarantees through distributed coordinate-free sensor activation," in *Proc. of MobiCom*, 2009.

[24] B. A. Bash and P. J. Desnoyers, "Exact distributed voronoi cell computation in sensor networks," in *SIAM Journal on Computing*, 2007.

[25] Y. Xu, J. Heidemann, and D. Estrin, "Geography-informed energy conservation for ad hoc routing," in *Proc. of MobiCom*, 2001.

[26] "GENI project." http://www.geni.net/.

[27] "Orbit." http://www.orbit-lab.org/.